*Sensors and Materials*, Vol. 35, No. 5 (2023) 1659–1670
MYU Tokyo



S & M 3278

# Application of Wireless Sensor Network Based on Improved Genetic Algorithm in Bridge Health Monitoring

Zhensong Ni,[1] Shuri Cai,[2*] and Cairong Ni[1]

[1]School of Big Data and Artificial Intelligence, Fujian Polytechnic Normal University,
No. 1, Campus New Village, Longjiang Street, Fuqing, Fujian Province 350300, China
[2]Institute of Highway Science, Ministry of Transport,
8 Xitucheng Road, Haidian District, Beijing 100086, China

(Received January 7, 2023; accepted April 26, 2023)

***Keywords:*** wireless sensor network, genetic algorithm, bridge inspection, degree of fitness

The optimal location and the number of sensors in the wireless sensor network were found efficiently and accurately using an improved genetic algorithm (IGA) and applied to the dynamic detection of bridges. First, we optimized the conventional genetic algorithm (GA) by considering the optimization characteristics of multiple sensors. IGA improves the drawbacks of the conventional GA, such as slow convergence and the tendency to fall into local optima when applied to large structures. This improvement increases the convergence speed and ensures an adequate search for the optimal value. To achieve the optimal arrangement, classical optimization criteria including the acceptable independence, model confidence, and model strain energy criteria are embedded into the IGA as fitness functions. Through the simulation analysis of a bridge model, we demonstrate that the IGA outperforms the conventional GA in terms of searching ability, computational efficiency, reliability, and other relevant metrics. Moreover, the IGA significantly outperforms the classical sequence method in the searching ability.

## 1. Introduction

To ensure the health of large bridges and other infrastructure, health monitoring systems and intelligent control technology have been developed rapidly and applied. Accordingly, the development of monitoring systems and control technology has attracted considerable research interest from researchers and engineers. Dynamic detection is an important approach for the diagnosis of the health of large bridges, and the results of dynamic detection largely depend on the locations and number of sensors. Therefore, it is of great theoretical value and practical significance to determine the optimal number and positions of sensors. To determine them, first, the optimal configuration criterion must satisfy the design requirements, and second, an appropriate optimization calculation must be performed. Recently, several optimization criteria and calculation methods have been suggested. Optimal configuration criteria based on model tests include(1) the model strain energy criterion,(2) the model reduction criterion,(3) and the model confidence criterion.(4)

*Corresponding author: e-mail: caishuri@126.com
https://doi.org/10.18494/SAM4309

ISSN 0914-4935 

The optimal configuration of sensors is established with sequence methods such as the step cutting method,[5] step accumulation method,[6] and random class methods that use the genetic algorithm (GA)[7] and simulated annealing.[8] At present, sequence methods are widely used but the calculation is complex, and only suboptimal solutions can be obtained. Therefore, we propose a measuring point optimization method with the improved GA (IGA) for the dynamic detection and monitoring of the health of large bridges. This algorithm is based on an adaptive and comprehensive cross-improvement to overcome the constraint conditions and defects of the conventional GA, which is slow to converge and easily falls into the local optima when applied to large structures. IGA has increased convergence speed and ensures the optimal value search. Classical optimization criteria such as the effective independence, model confidence, and model strain energy criteria are embedded into the IGA to obtain the optimal arrangement of sensors. Through the simulation analysis of a bridge model, we demonstrate that the IGA outperforms the conventional GA in terms of searchability, computational efficiency, and reliability. In particular, IGA's searchability is superior to that of the classical sequence method. In this study, three typical methods are selected and applied to bridge health monitoring. The model parameters and the mode shape of the structure are obtained using the response data collected from the actual sampling. In addition, haptic arrays for flexible sensor networks of the systems are applied to optimize the number and locations of sensors in the monitoring system. By using such sensor networks along with optimization algorithms, bridge health monitoring and infrastructure management can be carried out more effectively with IGA than with GA.

## 2. Point Optimization Principle Based on Improved Genetic Algorithm

Binary coding is adopted to optimize the number of sensors as the length of the binary code can be made equal to the optional position of the sensor as the node position in the finite element model without constraints. If the value of the *i*th node is 1, the sensor is arranged at the corresponding position. If it is 0, there is no sensor at the corresponding position. This coding method is intuitive and convenient for the following genetic operations. When generating the initial group of sensors, the differences between the two individual sensors must be known and the diversity of the initial group must be maintained as much as possible to meet the optimal condition.[9]

### 2.1 Fitness

Fitness is a measure of the degree to which each sensor in a group is likely to reach the optimal solution. In this study, the optimal allocation criterion reflecting the design requirements is taken as fitness.

#### 2.1.1 First fitness based on effective independence criterion (EIC)

Mattias *et al.* proposed the classical effective independence method, that is, the combination of the sequence method and the EIC. The principle is to optimize the Fisher information matrix

to keep the model vector of interest as linearly independent as possible and collect the maximum response information from the test data in the model.[10] According to this principle, we maximize the determinant of the Fisher information matrix Q as the search target. To facilitate the calculation, the fitness value is limited to be in an appropriate range and then optimized. Fitness $f$ is defined as

$$f = \log\left|\det\left(Q \times 10^{10}\right) \times 10^{-12}\right|. \tag{1}$$

### 2.1.2 Second fitness based on model confidence criterion (MAC)

According to the principle of structural dynamics, the values of the natural modes on the nodes form a set of orthogonal vectors. Pastor *et al.* believed that the model assurance criterion matrix (M-matrix) is an appropriate tool for evaluating the intersection angle of model vector space.[11] The related equation is expressed as

$$m_{ij} = \frac{\left|\phi_i^T \phi_j\right|^2}{\left|\phi_i^T \phi_i\right|\left|\phi_j^T \phi_j\right|}, \tag{2}$$

where $i$ and $j$ are mode vectors. By checking the off-diagonal elements of the M-matrix formed by each mode on the measured degree of freedom, the intersection of the corresponding two mode vectors can be judged. When a certain element of the M-matrix $M_{ij}$ ($i \neq j$) is equal to 1, the intersection angle of the $i$th and $j$th vectors is zero, and the two vectors cannot be distinguished. However, when $M_{ij}$ ($i \neq j$) is equal to zero, the two vectors are orthogonal and are easily identified. Therefore, the arrangement of measuring points must be minimized for the establishment of the off-diagonal elements of the M-matrix. Fitness $f$ is defined as

$$f = max\left(M\left(i, j\right)\right)\left(i \neq j\right). \tag{3}$$

### 2.1.3 Third fitness based on the model strain energy criterion (MKE)

The principle of this criterion is that the response of the degrees of freedom with large model strain energy also becomes large, and the sensor placement in these locations is conducive to parameter identification. In this criterion, the maximum strain energy at the selected location is the objective function,[12] and fitness $f$ is defined as

$$f = \sum_{i=1}^{n} \sum_{j=1}^{n} \sum_{r,s \in m} \left|\phi_{ri} k_{rs} \phi_{sj}\right|, \tag{4}$$

where $k_{rs}$ represents the stiffness influence coefficient between point $r$ and point $s$, $r$ and $s \in m$ are limited to all measuring points, and $n$ is the number of modes of concern.

### 2.2 Improved crossover operation

Crossover operation generates new offspring individuals (nodes) through gene replacement and recombination between parent individuals, which plays a key role in GA. During operation, the common cross-operation does not meet the condition of the fixed number of sensors. Therefore, a conditional two-point cross is adopted to solve this problem in this study. In the method, if the generated binary string meets the following conditions, Eq. (5) is obtained.

$$t_{(A)i} + t_{(A)i} + 1 + \cdots + t_{(A)j} = t_{(B)i} + t_{(B)i+1} + 1 + \cdots + t_{(B)j} \tag{5}$$

Here, if the gene values from $i$ to $j$ in the two parent individuals (A and B) are combined, new values from $i$ to $j$ are generated as offspring. If no such two parent points can be found, an individual supplementary offspring meeting the initial conditions is randomly generated.

### 2.3 Mutation and calculation

Mutation operation is beneficial to prevent immature convergence. Here, different gene values are swapped, that is, a gene position with code values 1 and 0 is randomly selected. Then, code values are exchanged at the two positions. In binary coding, the crossover rate of 1 is used to calculate the fitness of the offspring and the parent generation, and the number of the former population is taken as the next generation according to the fitness. In this way, the random selection of the crossover significantly increases the convergence speed compared with the conventional GA. To prevent immature convergence, adaptive selection variation is adopted. When the search develops along the fast optimization direction, a small variation rate is adopted to carry out one variation transformation. When several consecutive values are constant, a large variation rate is adopted and multiple variation transformations are carried out. The above improvements make the algorithm converge rapidly, but it is not easy to fall into the local optima. In actual operations, individuals with the greatest fitness can be directly entered into the next generation to maintain growth. To ensure the reliability of the algorithm, the optimal value is calculated continuously 16 times.

## 3. Improved Genetic Algorithm for Sensor Position Optimization

The bridge produces a dynamic response to wind and vehicle loads. Its vibration characteristics are analyzed by measuring the response, providing data for damage identification and model correction. Therefore, to diagnose the health of the structure, especially of the cable-stayed bridge, the acceleration of key parts should be measured. According to the existing conditions of the Jintang Bridge in Zhejiang, China, we use wireless acceleration sensors to detect the acceleration of the bridge deck.[13,14]

To optimize the layout of 26 sensors and ensure the optimization, MATLAB is used to test GA and IGA in simulation. The arrangement of sensors with EIC combined with the sequence method (SSP) is compared with the simulation result to calculate the equivalent fitness values.

The fitness values of GA, IGA, and SSP are compared in Table 1. In terms of the optimal and average values, IGA is superior to GA, indicating that IGA has a strong searching ability. The standard deviation of IGA is small, indicating good reliability. In addition, IGA saves about two-thirds of the computing time. The locations of 26 acceleration sensors on the bridge deck are proposed according to the optimal fitness results calculated according to each criterion.

To assess the effects of different criteria on parameter identification, the output response of measuring points is extracted under white noise excitation using ANSYS. The natural excitation technique (NEXT) and eigensystem realization algorithms (ERAs) are applied to find structural model parameters of the response data. The difference between the recognized and real mode shapes is expressed by model confidence (MAC value), the definition of which is Eq. (2).[15,16] For the convenience of comparison, the MAC values of the identified and theoretical mode shapes of the finite element model are listed together with the results of the mode shapes based on the field data and the MAC values of the theoretical mode shapes. The results are shown in Table 2.

On the whole, the first and second vertical mode shapes and the first torsional mode shapes are identified by fewer sensors on the basis of the above criteria, and the first transverse mode shapes are well identified. The three layout schemes with different criteria meet the detection requirements and show satisfactory accuracy of identification and optimization. Simulation results show that IGA has an advantage over the mature sequence method in mode recognition and maintains this advantage in an application, especially in the recognition of the torsional second-order mode. The values of the high-order mode shapes obtained by the analysis of the measured data are different from the theoretical values and those of the mode shapes. The difference mainly is caused by the data loss of four measurement points.

In the actual monitoring system, individual sensor failures are found often owing to the sensor performance, durability, construction, environmental impact, and aging of the system. Therefore, it is necessary to evenly arrange sensors to avoid the effects of such causes on the whole monitoring result.

Table 1
Comparison of fitness between GA and IGA.

| Method | EIC | | | MAC | | MKE | |
|---|---|---|---|---|---|---|---|
| | GA | IGA | SSP | GA | IGA | GA | IGA |
| 1 | 103.22 | 103.3 | 99.345 | 0.22005 | 0.21834 | 189.91 | 189.96 |
| 2 | 103.18 | 103.22 | | 0.21746 | 0.217 | 189.96 | 189.96 |
| 3 | 103.28 | 103.3 | | 0.2185 | 0.21927 | 189.95 | 189.95 |
| 4 | 103.22 | 103.3 | | 0.21797 | 0.21767 | 189.96 | 189.96 |
| 5 | 103.05 | 103.34 | | 0.21771 | 0.21699 | 189.87 | 189.96 |
| 6 | 103.25 | 103.34 | | 0.22119 | 0.21932 | 189.96 | 189.93 |
| 7 | 103.21 | 103.32 | | 0.21714 | 0.21984 | 189.83 | 189.96 |
| 8 | 103.3 | 103.31 | | 0.22323 | 0.21774 | 189.96 | 189.91 |
| 9 | 103.29 | 103.34 | | 0.21774 | 0.21874 | 189.91 | 189.96 |
| 10 | 103.28 | 103.34 | | 0.22339 | 0.21807 | 189.96 | 189.96 |
| Mean value | 103.23 | 103.31 | — | 0.21944 | 0.2183 | 189.93 | 189.95 |
| Variance | 0.074057 | 0.036652 | — | 0.002393 | 0.00098418 | 0.0462 | 0.017288 |
| Optimum | 103.29 | 103.34 | 99.345 | 0.21714 | 0.21699 | 189.96 | 189.96 |

Table 2
Comparison of MAC values of mode shapes under different sensor placements.

| Order of mode shape | EIC | | | | MAC | | | | MKE | | | |
|---|---|---|---|---|---|---|---|---|---|---|---|---|
| | Simulation and theoretical recognition values | | Experimental and theoretical identification values | | Simulation and theoretical recognition values | | Experimental and theoretical identification values | | Simulation and theoretical recognition values | | Experimental and theoretical identification values | |
| | Lateral | Vertical | Lateral | Vertical | Lateral | Vertical | Lateral | Vertical | Lateral | Vertical | Lateral | Vertical |
| 1 | 0.9991 | 0.9499 | 0.9357 | 0.9778 | 0.9988 | 0.9611 | 0.9895 | 0.9856 | 0.9987 | 0.9614 | 0.9562 | 0.9840 |
| 2 | 0.8487 | 0.9950 | — | 0.9422 | 0.9407 | 0.9958 | — | 0.9705 | 0.9016 | 0.9954 | — | 0.9761 |
| 3 | 0.6976 | 0.9204 | — | — | 0.6075 | 0.9155 | — | — | 0.7784 | 0.8904 | — | — |
| 4 | 0.7856 | 0.91092 | — | — | 0.2515 | 0.9058 | — | — | 0.3969 | 0.9146 | — | — |
| 5 | 0.0078 | 0.99132 | — | — | 0.00105 | 0.9938 | — | — | 0.00122 | 0.9909 | — | — |
| 6 | 0.5340 | 0.96629 | — | — | 0.1319 | 0.9243 | — | — | 0.5266 | 0.9601 | — | — |
| 7 | — | 0.99141 | — | — | — | 0.9644 | — | — | — | 0.9914 | — | — |
| 8 | — | 0.97519 | — | 0.8619 | — | 0.9535 | — | 0.9721 | — | 0.9752 | — | 0.9826 |
| 9 | — | 0.98077 | — | — | — | 0.9804 | — | 0.9531 | — | 0.9808 | — | 0.8854 |
| 10 | — | 0.98414 | — | — | — | 0.7208 | — | — | — | 0.9903 | — | — |
| 11 | — | 0.33158 | — | — | — | 0.3080 | — | — | — | 0.4320 | — | — |
| 12 | — | 0.00066 | — | — | — | 0.9289 | — | — | — | 0.2087 | — | — |

## 4. Computation Method

Midas Civil structural analysis software is used to determine the loading for the simulation. The calculation model is shown in Fig. 1. The discrete steel box girder and cable tower are beam elements, and the discrete stay cable is a truss element.

### 4.1 Load test conditions

A static load test is used to simulate the internal force generated by a three-axle truck weighing of about 300 kN as the equivalent load. The number of vehicles to be loaded is based on Zhejiang Province's guidelines on "Standardizing Bridge Loads and Pile Test Behaviors". The principles of the guidelines are as follows.

$$0.90 \le \eta = \frac{S_{stat}}{(1+\mu)\cdot s} \le 1.05 \tag{6}$$

Here, $\eta$ is the efficiency of the static load test, $S_{stat}$ is the maximum value on the internal force or by the displacement of the control section, $s$ is the most unfavorable value generated by the standard load without the impact load, and $(1 + \mu)$ is the impact factor used in the test and calculation.

For simulation, we adopt working conditions 8 and 15. Working condition 8 assumes the maximum positive bending moment and deflection of steel box girder D3-D4 pier L/2 section (H section) under the most unfavorable cable force increment in the middle span (symmetrical distribution and partial loads). Working condition 15 is for the loading test of the maximum local stress for the side and middle span 3# cables. The test load efficiency is shown in Table 3.

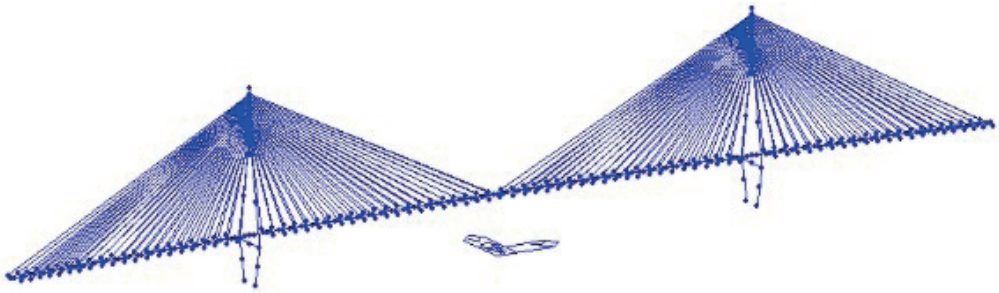

Fig. 1. (Color online) 3D finite element model of Jintang Bridge in Zhoushan.

Table 3
Loading efficiency of static load test.

| Working condition | Test item | Loading position | Calculation | Effect design | Effect load efficiency |
|---|---|---|---|---|---|
| 8 | Maximum cable force increment of 21# side span | Symmetrical distribution load | 619.21 | 636.61 | 0.97 |
| | | Partial load | 472.95 | 518.86 | 0.91 |
| | Maximum cable force increment of 21# cable in the middle span | Symmetrical distribution load | 555.60 | 617.33 | 0.90 |
| | | Partial load | 423.65 | 470.72 | 0.90 |
| 15 | Maximum cable force increment for side and middle span 3# cables | Symmetrical distribution load | Side span | 215.94 | |
| | | | Middle span | 220.09 | |

Note: The unit of bending moment in the table is KN-m, the unit of shear, cable, and reaction forces is KN, and the unit of deflection is m.

### 4.2 Cable force incremental test results

Under a full load of working condition 8, the incremental verification coefficient of cable tension of JB21 and JZ21# is measured as between 0.73 and 1.03, and the measured incremental value is less than or close to the calculated value. This result indicates that the working condition of the cable meets the design requirements. Figure 2 shows the cable force test results, and the detailed test analysis results are presented in Table 4.

### 4.3 Measurement results of vibration characteristics

The parameters of vibration characteristics of the bridge structure include vibration frequency, mode shape, and damping ratio. They are the determinants of the dynamic performance of a bridge and characterize the overall state of the structure. Many technical problems of the bridge are closely related to the dynamic characteristics of its structure, such as the structural problem, wind resistance, and seismic performance. The vibration test of a bridge is performed with wireless servo acceleration sensors to assess the pulsation of the main beam. The main tower is tested in the wired mode owing to signal problems. The natural pulsation test method is used to obtain the natural vibration parameters and measure the small vibration of the bridge structure caused by random loads such as wind load, ground pulsation, and water flow assuming no traffic load on the bridge deck and no regular vibration source near the bridge.

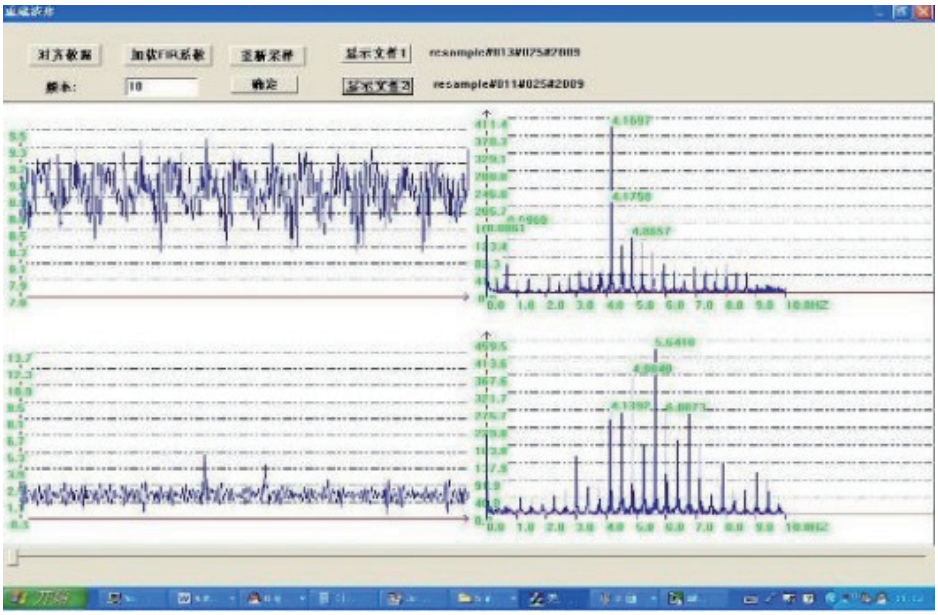

Fig. 2. (Color online) Cable force test result with a full load of working condition 8 in Jintang Bridge.

Table 4
Test results of cable force increment in working condition 8.

| Working condition | Line no. | Measured cable force increment (kN) | Calculated cable force increment (kN) | Checkout coefficient |
|---|---|---|---|---|
| Working condition 8, medium load | JB21 #right side | 532 | 619 | 0.86 |
| | JB21 #left side | 472 | 619 | 0.76 |
| | JZ21 #right side | 526 | 556 | 0.95 |
| | JZ21 #left side | 518 | 556 | 0.93 |
| Operating condition 8, off-load | JB21 #right side | 415 | 473 | 0.88 |
| | JB21 #left side | 318 | 350 | 0.91 |
| | JZ21 #right side | 437 | 424 | 1.03 |
| | JZ21 #left side | 229 | 313 | 0.73 |

Notes: 1. Ningbo direction to distinguish between left and right; 2. offset load position is arranged on the right side; 3. cable force is increased positively.

By measuring the vibrations of the bridge tower, steel box girder, and stay cable caused by environmental factors, the dynamic parameters of the vibrations of the bridge are identified, including vibration frequency, vibration mode, and damping ratio. The vibration mode reflects the vertical, transverse, and longitudinal vibrations of the bridge, and the bending and torsional modes are obtained for the steel beam and cable tower.

To obtain a complete shape curve, 69 test sections and seven test sections in each pylon body are set on the test deck. In the test, the 16-order natural vibration modes of the bridge are obtained. The actual vibration modes and frequencies are shown in Table 5 and Figs. 3–10. The theoretical calculation result shows that the measured vibration frequency of the first-order cable tower and steel box girder combined with longitudinal drift is 0.10 Hz, which is slightly lower than the calculated value of 0.111 Hz. The measured vibration frequency of other orders is higher than the corresponding calculated value.

Table 5
Test results of structural natural vibration characteristic parameters.

| Serial number | Description of mode shape | Measured frequency (Hz) | Calculation frequency (Hz) |
|---|---|---|---|
| 1 | Cable tower and steel box girder float together | 0.10 | 0.111 |
| 2 | Steel box girder has one transverse bend in middle span and side span | 0.23 | 0.193 |
| 3 | Vertical bend of middle span and side span of steel box girder is combined with longitudinal deflection of cable tower | 0.28 | 0.222 |
| 4 | Secondary vertical bend of middle span and primary vertical bend of side span are combined with longitudinal deflection of cable tower | 0.34 | 0.287 |
| 5 | Secondary transverse bend of middle span and primary transverse bend of side span are combined with transverse deflection of cable tower | 0.53 | 0.530 |
| 6 | Steel box girder combines three vertical bends in middle span and one vertical bend in side span | 0.55 | — |
| 7 | Four vertical bends of middle span and one vertical bend of side span of steel box girder are combined with longitudinal deflection of cable tower | 0.58 | — |
| 8 | Secondary transverse bend of middle span and primary transverse bend of side span are combined with transverse deflection of cable tower | 0.67 | 0.635 |
| 9 | Four vertical bends of middle span and one vertical bend of side span of steel box girder are combined with longitudinal deflection of cable tower | 0.74 | 0.585 |
| 10 | Steel box girder combines four vertical bends in middle span and one vertical bend in side span | 0.82 | 0.663 |
| 11 | Steel box girder has one torsion in middle span | 0.87 | 0.613 |
| 12 | Fifth vertical bend of middle span of steel box girder combined with longitudinal deflection of steel box girder | 0.92 | — |
| 13 | Steel box girder combines six vertical bends in middle span and one vertical bend in side span | 0.96 | — |
| 14 | Steel box girder combines six vertical bends in middle span, two vertical bends in secondary side span, and one vertical bend in side span | 1.04 | 0.766 |
| 15 | Steel box girder has seven vertical bends in middle span | 1.16 | 0.802 |
| 16 | Steel box girder has eight vertical bends in middle span | 1.60 | 1.139 |

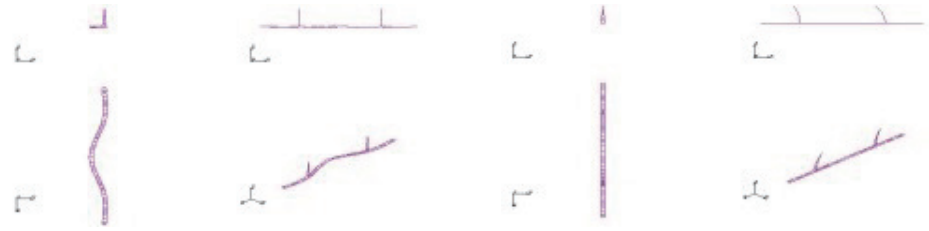

(a) (b)

Fig. 3. (Color online) Diagrams of (a) first-order and (b) second-order modes.

(a) (b)

Fig. 4. (Color online) Diagrams of (a) third-order and (b) fourth-order modes.

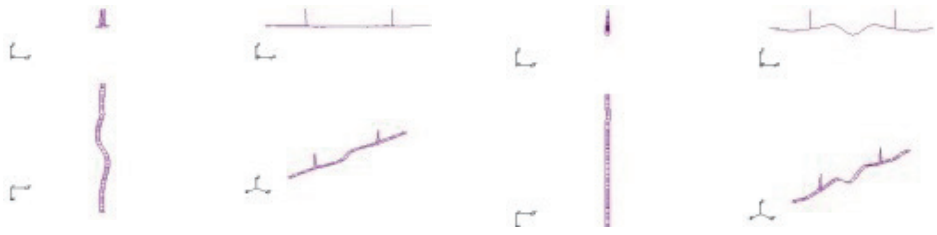

(a) (b)

Fig. 5. (Color online) Diagrams of (a) fifth-order and (b) sixth-order modes.

(a) (b)

Fig. 6. (Color online) Diagrams of (a) seventh-order and (b) eighth-order modes.

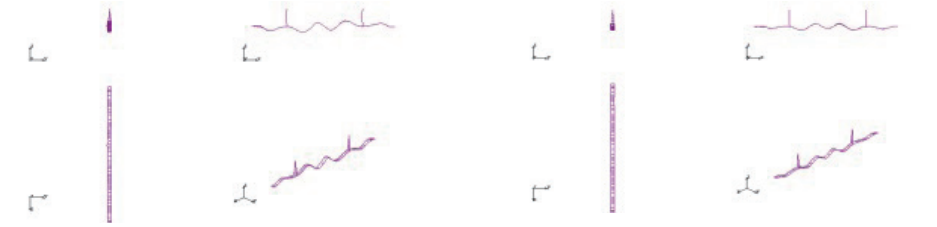

(a) (b)

Fig. 7. (Color online) Diagrams of (a) ninth-order and (b) tenth-order modes.

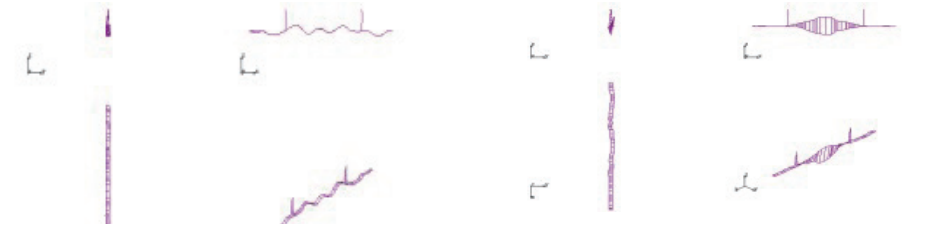

(a) (b)

Fig. 8. (Color online) Diagrams of (a) eleventh-order and (b) twelfth-order modes.

(a) (b)

Fig. 9. (Color online) Diagrams of (a) thirteenth-order and (b) fourteenth-order modes.

(a) (b)

Fig. 10. (Color online) Diagrams of (a) fifteenth-order and (b) sixteenth-order modes.

## 5. Conclusions

In the bridge health monitoring system, the damage identification and safety assessment of the structure need a model test to obtain the optimal model parameters. In the model test, the number of sensors and their locations in the structure are important for obtaining accurate parameters. To optimize the sensor layout of the Jintang Bridge, GA, and IGA are compared to understand vibration characteristics on the basis of three different criteria. The spatial finite element method is used to perform the test with 26 wireless acceleration sensors installed on the bridge to collect data for the comparison of the results of GA and IGA. The data are used to analyze the optimal fitness to propose the optimal locations of the sensors by measuring the vibration frequency. The result shows that IGA has a stronger searching ability, a higher reliability, and a faster computing time than GA. In particular, IGA is effective in measuring the vertical displacement and longitudinal strain of the main beam of the bridge and the longitudinal inclination of the tower. IGA effectively improves the calculation of the algorithm by introducing the adaptive genetic operator and multi-objective function.

## Acknowledgments

This study was supported by the Natural Science Foundation of Fujian Province (2018J0106) and the phased research result of the provincial major research project on education and teaching reform of undergraduate colleges and universities in Fujian Province [project name: Research on Three Innovation Education Projects of Internet of Things Engineering (project no. fbjg202101018)].

## References

1 T.-H. Li, H.-N. Li, and X.-D. Zhang: Struct. Control Health Monit. **22** (2015) 123. https://doi.org/10.1002/stc.1664
2 S. A. H. Kordkheili, S. H. M. Massouleh, S. Hajirezayi, and H. Bahai: J. Sound Vibr. **412** (2018) 116. https://doi.org/10.1016/j.jsv.2017.09.038
3 Y. Chen: Mech. Syst. Signal Process. **151** (2021) 107363. https://doi.org/10.1016/j.ymssp.2020.107363
4 H. Yin, Y. Zhang, and X. He: Algorithms **11** (2018)147. https://doi.org/10.3390/a11100147
5 J.-F. Lin, Y.-L. Xu, and S.-S. Law: J. Sound Vib. **422** (2018) 568. https://doi.org/10.1016/j.jsv.2018.01.047
6 L. Vincenzi and L. Simonini: J. Sound Vib. **389** (2017) 119. https://doi.org/10.1016/j.jsv.2016.10.033
7 M. Nasir, A. Rehman Javed, M. Adnan Tariq, M. Asim, and T. Baker: J. Supercomput. **78** (2022) 8852. https://doi.org/10.1007/s11227-021-04250-0

8 X. Zhu, D. Xingxia, J. Hongbo, W. Dong, C. Hongyang, Y. Liang, and Z. Fanzi: IEEE Internet Things J. **7** (2020) 2038. https://doi.org/10.1109/jiot.2019.2960631
9 G.-D. Zhu, T.-H. Yi, M.-X. Xie, and H.-N. Li: Smart Mater. Struct. **26** (2017) 104002. https://doi.org/10.1088/1361-665X/aa7930
10 R. Mattias, K. Bertram, K. Martina, and B. Nils: Nucleic Acids Res. **48** (2020) 307. https://doi.org/10.1093/nar/gkaa236
11 M. Pastor, M. Binda, and T. Harčarik: Procedia Eng. **48** (2012) 543. https://doi.org/10.1016/j.proeng.2012.09.551
12 T. Kim, B. Youn, and H. Oh: Mech. Syst. Signal Process. **111** (2018) 615. https://doi.org/10.1016/j.ymssp.2018.04.010
13 S. Weiwei, S. Liang, S. Hu, and L. Pengjie: Int. J. Appl. Mat. Comput. Sci. **31** (2021) 271. https://doi.org/10.34768/AMCS-2021-0019
14 E. Yakick and M. Karatas: Comput. Netw. **192** (2021) 108041. https://doi.org/10.1016/j.comnet.2021.108041
15 E. Neu, F. Janser, A. A. Khatibi, and A. C. Orifici: Mech. Syst. Signal Process. **84** (2017) 308. https://doi.org/10.1016/j.ymssp.2016.07.031
16 S. Parsa, C. Samson, and S. Omar: Resour. Conserv. Recycl. **173** (2021) 105701. https://doi.org/10.1016/J.RESCONREC.2021.105701

## About the Authors

**Zhensong Ni** received his bachelor's degree from Fuzhou University in 1995, his master's degree from Beijing Information Science and Technology University in 2007, and his doctorate degree from Beijing University of Posts and Telecommunications in 2010. From 2010 to 2012, he was a lecturer at Tianjin Polytechnic University, from 2012 to 2014, he was an assistant professor at Tsinghua University, and since 2014, he has been an associate professor at Fujian Normal University of Technology. His research interests include MEMS, big data, and sensors. (460532802@qq.com)

**Shuri Cai** received his bachelor's degree from Fujian Normal University in 1997 and his master's and doctorate degrees from Beijing University of Posts and Telecommunications, China, in 2004 and 2008, respectively. Since 2007, he has worked as an associate researcher at the Institute of Highway Science under the Ministry of Transport. His research interests include MEMS, big data, and sensors. (caishuri@126.com)

**Cairong Ni** received his bachelor's degree from Sunshine College in 2022. He has been working as a teaching assistant at Fujian Normal University of Technology since 2022. His research interests include MEMS, big data, and sensors. (3247146792@qq.com)